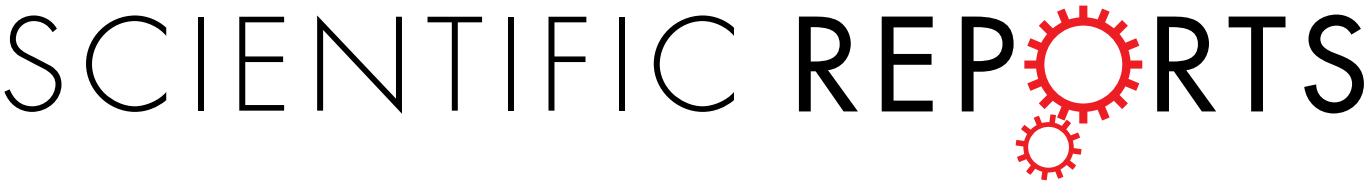

OPEN

Nonlinear plasmonic dispersion and coupling analysis in the symmetric graphene sheets waveguide

Received: 14 June 2016
Accepted: 22 November 2016
Published: 15 December 2016

Xiangqian Jiang, Haiming Yuan & Xiudong Sun

We study the nonlinear dispersion and coupling properties of the graphene-bounded dielectric slab waveguide at near-THz/THz frequency range, and then reveal the mechanism of symmetry breaking in nonlinear graphene waveguide. We analyze the influence of field intensity and chemical potential on dispersion relation, and find that the nonlinearity of graphene affects strongly the dispersion relation. As the chemical potential decreases, the dispersion properties change significantly. Antisymmetric and asymmetric branches disappear and only symmetric one remains. A nonlinear coupled mode theory is established to describe the dispersion relations and its variation, which agrees with the numerical results well. Using the nonlinear couple model we reveal the reason of occurrence of asymmetric mode in the nonlinear waveguide.

At THz and far-infrared frequency range, the electrons transition of intraband dominates primarily and the metallic conductivity of Drude type makes the graphene surface plasmon be supported. Based on its unique electric and optical properties[1] graphene has been suggested as an alternative to conventional metal-based structures to confine light and guide surface plasmon polaritons. Electromagnetic properties of graphene-dielectric composite structures have attracted special attention in the past years, leading to the rapid development of a new branch of plasmonics known as graphene plasmonics[2–5].

Considerable effort has been devoted to investigating the mode propagation[6–10], localization[11,12] and coupling[13–21] of graphene plasmon in the linear graphene-dielectric composite structures. The propagation properties of guided graphene plasmon in individual and paired graphene ribbons were studied[6], and the features of low loss, large confinement of light and flexible tunability were found. To manipulate the energy flow of light, Wang *et al.*[7] proposed a graphene plasmonic lens[7], this lens can be used to focus and collimate the graphene plasmon waves propagating along the graphene sheet. The confinement of plasmon in very small regions has potential applications in optoelectronics, the surface plasmon resonance in graphene sub-nanometre scale has been explored[11].

The coupling effects of graphene plasmon have attracted wide interest. The demonstration of surface plasmon excitation in graphene based on the near-field scattering of infrared light has been reported[13,14]. Recently, Constant *et al.*[15] presented an all-optical plasmon coupling scheme which takes advantage of the intrinsic nonlinear optical response of graphene, and found that surface plasmons with a defined wavevector and direction can be excited by controlling the phase matching conditions. To realize ultra-high contrast optical modulators, the phase-coupling scheme of localized graphene plasmon resonances has been proposed to replace the original near-field coupling[17]. Moreover, the tunable multiple plasmon induced transparencies based on phase-coupling has been demonstrated by the same group[18]. For the graphene-dielectric multilayer structure, the mode coupling properties and its control are useful for designing compact and tunable nanophotonic devices. It is shown that the graphene-dielectric-graphene waveguide can support both symmetric and antisymmetric modes[19,20]. When the graphene sheets are arranged periodicly and tightly, the strong coupling between surface plasmon polaritons emerges[21].

As was shown, graphene is a strongly nonlinear material[22,23]. Several nonlinear optical effects based on graphene's nonlinearity were predicted[24–28]. A novel class of nonlinear self-confined modes originated from the hybridization of surface plasmon polaritons with graphene optical soliton is demonstrated to exist in graphene monolayers[25]. In order to increase the nonlinearity of photonic structures with graphene, the graphene multilayer structure is presented. The nonlinear switching and palsmon soliton based on graphene multilayer were demonstrated[26,27]. For the nonlinear graphene-dielectric-graphene structure[26], the symmetric, antisymmetric and asymmetric mode were found in the structure. The occurrence of asymmetric mode means the symmetry breaking

Department of Physics, Harbin Institute of Technology, Harbin 150001, China. Correspondence and requests for materials should be addressed to X.J. (email: xqjiang@hit.edu.cn)

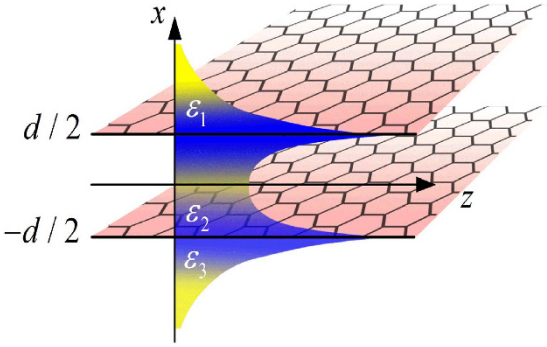

Figure 1. Schematic diagram of nonlinear symmetric graphene sheets plasmonic waveguide, $\varepsilon_1 = \varepsilon_3 = 1$, $\varepsilon_2 = 2.25$.

phenomenon. However, the mechanism of symmetry breaking is still unclear although the phenomenon was found in nonlinear plasmonic waveguides. Therefore, the purpose of this article is to study nonlinear plasmonic dispersion and coupling properties in symmetric graphene sheets waveguide, and reveal the mechanism of symmetry breaking phenomenon.

Results

Nonlinear modes and dispersion properties. The nonlinear graphene plasmonic waveguide is illustrated in Fig. 1. The dielectric slab waveguide of ε_2 is bounded by the graphene layers at $x = \pm d/2$ with the surrounding dielectric ($\varepsilon_1 = \varepsilon_3$). According to the Kubo formula[29], the linear conductivity of grapheme σ_L contains the interband and intraband transition contributions. In the THz and far-infrared frequency range, the intraband transition dominates the linear conductivity of graphene which can be reduced to the Drude form[29]

$$\sigma_L = \sigma_{\text{intra}} = \frac{e^2\mu_c}{\pi\hbar^2}\frac{i}{\omega + i\tau^{-1}} \tag{1}$$

where e is the electron charge, μ_c is the chemical potential of graphene, ω is the frequency, and τ is the momentum relaxation time. This model is applicable in low temperature limit ($k_B T \ll \mu_c$) at low frequency ($\hbar\omega \le \mu_c$).

For the strong field condition, the nonlinear part of the conductivity must be considered and the total conductivity of graphene reads[27]

$$\sigma_g = \sigma_L + \sigma^{NL}|E_\tau|^2 \tag{2}$$

where E_τ is the tangential component of the electric field and σ^{NL} denotes nonlinear conductivity

$$\sigma^{NL} = -i\frac{3}{8}\frac{e^2}{\pi\hbar^2}\left(\frac{e\nu_F}{\mu_c\omega}\right)^2\frac{\mu_c}{\omega} \tag{3}$$

where $\nu_F = 0.95 \times 10^8$cm/s is the Fermi velocity.

Considering the transverse-magnetic (TM) surface plasmon polaritons mode that propagates along z direction with a propagation constant β, the magnetic and electric field should be in the form of $\mathbf{H} = H_{\pm,y}\exp(i\beta z \pm K_x x)\hat{\mathbf{y}}$ and $\mathbf{E} = (E_{\pm,x}\hat{\mathbf{x}} + E_{\pm,z}\hat{\mathbf{z}})\exp(i\beta z \pm K_x x)$ in the dielectrics or air, respectively, where $K_x = (\beta^2 - k_0^2\varepsilon)^{1/2}$ and $k_0 = \omega/c$. According to the boundary condition, the tangential component of electric field must be continuous while that one of the magnetic field has a discontinuity of $\sigma_g E_{1,+,z}$, i.e.,

$$\begin{aligned} &E_{2,+,z}e^{-K_{2,x}d} + E_{2,-,z} - E_{1,+,z} = 0 \\ &H_{2,+,y}e^{-K_{2,x}d} + H_{2,-,y} - H_{1,+,y} = \sigma_g E_{1,+,z} \end{aligned} \tag{4}$$

'±' in the subscript represents the field decrease and increase along upward direction of x. Similar boundary condition was also established at lower boundary. The Maxwell equation gives the relation

$$H_{\pm,y} = \pm E_{\pm z}\frac{\omega\varepsilon_0\varepsilon}{iK_x} \tag{5}$$

Applying Eq. (5) to region 1, 2 and 3, the dispersion relation equation was obtained with unknown variations of (β,ω,$H_{1,-z} \equiv H_0$).

Dependence of the magnetic field H_0 on the propagation constant β at wavelength $\lambda = 10\,\mu$m is shown in Fig. 2, where other parameters are fixed to the values $d = 100$ nm, $\varepsilon_1 = 1$, $\varepsilon_2 = 2.25$, $\mu_c = 0.27$ eV and $\tau = 1.5$ ps. The propagation constant β is normalized by Fermi vector $k_F = (\pi n)^{1/2}$[30] with the carrier density of $n = 6 \times 10^{12}$ cm^{-2}. There are three modes in the nonlinear plasmonic waveguide, which are symmetric mode, antisymmetric mode and asymmetric mode[26]. However, it is impossible to distinguish which branch denotes symmetric, antisymmetric

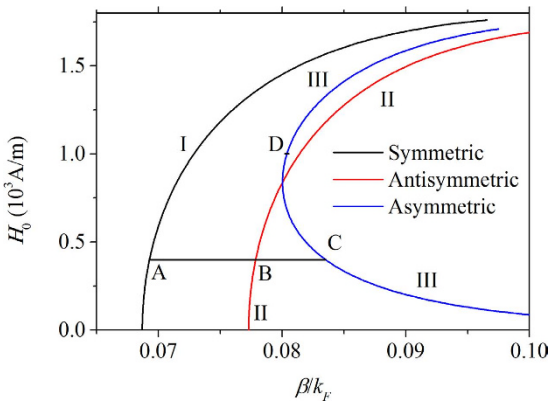

Figure 2. The initial magnetic intensity versus the propagation constant for the fixed wavelength $\lambda = 10\,\mu$m, the horizontal black solid line is an auxiliary line.

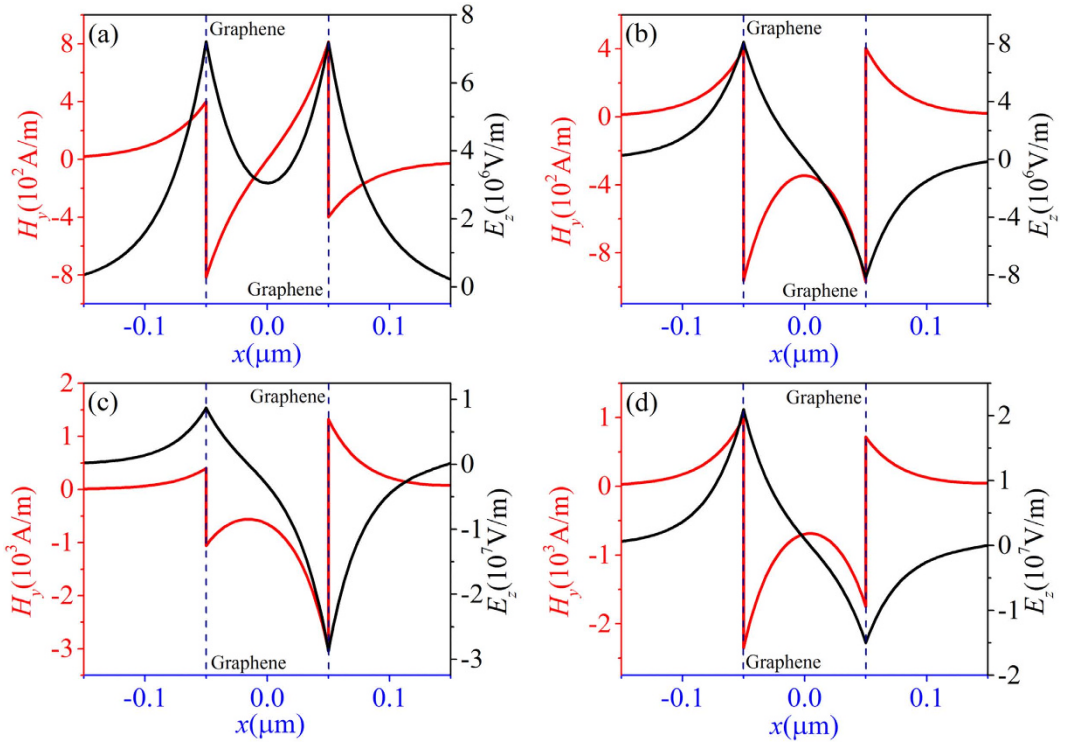

Figure 3. The field distribution for magnetic component H_y and electric component E_z, which correspond to points A, B, C and D in Fig. 2, respectively. (**a**) $(H_0, \beta) = (400\text{A/m}, 0.0779k_F)$, (**b**) $(H_0, \beta) = (400\text{A/m}, 0.0693k_F)$, (**c**) $(H_0, \beta) = (400\text{A/m}, 0.0835k_F)$, (**d**) $(H_0, \beta) = (1000\text{A/m}, 0.0805k_F)$. Other parameters are the same as in Fig. 2.

or asymmetric mode. To verify the mode properties of these branches in Fig. 2 we plot electric field and magnetic field distribution associated with A, B, C and D, respectively.

For branch I the fields are plotted in Fig. 3(a), in which distribution of electric field E_z is a symmetric. Therefore, the branch I represents the symmetric mode. For branch II distribution of electric field E_z shown in Fig. 3(b) is antisymmetric. It corresponds to the antisymmetric mode. The branches I and II represent symmetric and antisymmetric modes with respect to the linear conditions. They are caused by coupling of graphene plasmon on the upper and the lower air/graphene/dielectric interfaces. Another branch III is a novel mode which appears only due to nonlinearity. It yields to an interesting field distributions associated with C and D at branch III which are plotted in Fig. 3(c) and (d). Corresponding field distribution is asymmetric, and therefore branch III represents asymmetric mode.

Next, we turn our attention to discuss the influence of nonlinearity of graphene on dispersion relation. In Fig. 4, the dispersion relations are depicted with the dotted curves in linear case ($\sigma^{NL} = 0$) and by the solid curves

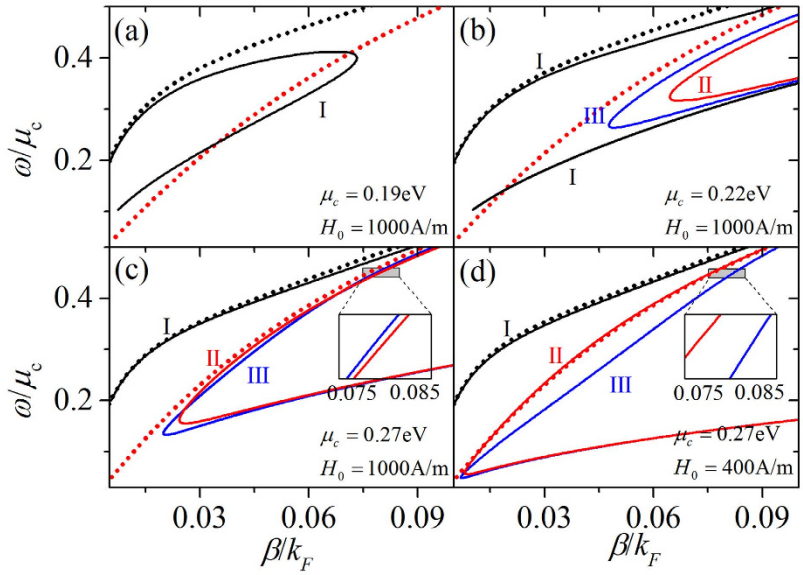

Figure 4. The dispersion relations for various nonlinearity of graphene. The dotted curves represent the dispersion relation of linear case, and the solid curves denote the dispersion relation of nonlinear case. The parameters (μ_c, H_0) are chosen to (**a**) (0.19 eV, 1000A/m); (**b**) (0.22 eV, 1000A/m); (**c**) (0.27 eV, 1000A/m); (**d**) (0.27 eV, 400A/m).

in nonlinear case. For the linear case only symmetric and antisymmetric modes exist. The black dotted curve and the red dotted curve represent the symmetric and antisymmetric modes, respectively. In Fig. 4(a–c) dispersion relation for fixed initial magnetic field ($H_0 = 1000$ A/m) and different chemical potentials μ_c is given. As is shown in Fig. 4(a), for the larger nonlinearity, when $\mu_c = 0.19$ eV, only symmetric mode represented by the solid curve is found. It is seen from Fig. 4(b) that at chemical potential is equal to 0.22 eV, antisymmetric (red solid curve) and the asymmetric (blue solid curve) modes appear in addition to symmetric mode of branch I. Further increase chemical potentia l ($\mu_c = 0.27$ eV) leads to the intersection of antisymmetric and asymmetric modes, which is seen in Fig. 4(c). In Fig. 4(d), these results are compared to those obtained at constant value of chemical potential $\mu_c = 0.27$ eV, and to decreased initial magnetic field H_0. Decrease of H_0 leads to consequent reduction of nonlinearity of graphene. In this case the fold-back point of the dispersion relations moves down. In addition, as is shown in Fig. 2, there is a intersection of the antisymmetric and asymmetric branch. Therefore, red and blue modes show an opposite trend when the wavelength of the insets in Fig. 4(c) and (d) is about 10 μm ($\omega/\mu_c = 0.45$). The lower branch of mode I is not plotted in Fig. 4(c) and (d), since it is too close to the lower branch of mode II and III. Nevertheless, it exists.

Nonlinear coupled mode theory. In the case of weak field without nonlinearity, the coupled graphene plasmonic waveguide shown in Fig. 1 are depicted in Fig. 5(a). According to the coupled mode theory[31], the oscillation energies a_1 and a_2 satisfy the matrix equation

$$\begin{pmatrix} i\beta_1 & i\kappa \\ i\kappa & i\beta_2 \end{pmatrix} \begin{pmatrix} a_1 \\ a_2 \end{pmatrix} = \frac{\partial}{\partial z} \begin{pmatrix} a_1 \\ a_2 \end{pmatrix} \tag{6}$$

where β_1 and β_2 are the propagation constants of the single layer graphene waveguide without coupling and κ is the coupling coefficient. The weak field condition of symmetric structure without nonlinearity corresponds to $\beta_1 = \beta_2 = \beta_0$. The propagation constants of the coupled mode are defined as the eigenvalues of the matrix

$$\beta_\pm = \beta_0 \pm \kappa \tag{7}$$

They could also be obtained from the mode analysis method. Figure 5(b) presents the dispersion relations of the same structure as is shown in Fig. 1. In this case the coupling coefficient is found to be $\kappa = 4.3 \times 10^{-3} k_F$ at wavelength $\lambda = 10\,\mu$m.

When the graphene's nonlinearity is considered, the propagation constant of each single graphene waveguide becomes a function of tangential component of electric field. The dispersion of the single graphene waveguide is[32]

$$\frac{\varepsilon_1}{K_{x,1}} + \frac{\varepsilon_2}{K_{x,2}} - \frac{\sigma}{i\omega\varepsilon_0} = 0 \tag{8}$$

where $K_{x,1,2} = (\beta^2 - k_0^2 \varepsilon_{1,2})^{1/2}$. Substituting Eq. (2) into Eq. (8) one gets the nonlinear propagation constant of the single layer graphene waveguide which is shown in Fig. 5(c). Replacing β_1 and β_2 in Eq. (6) with $\beta_{1,2}(|E_z|^2)$ and

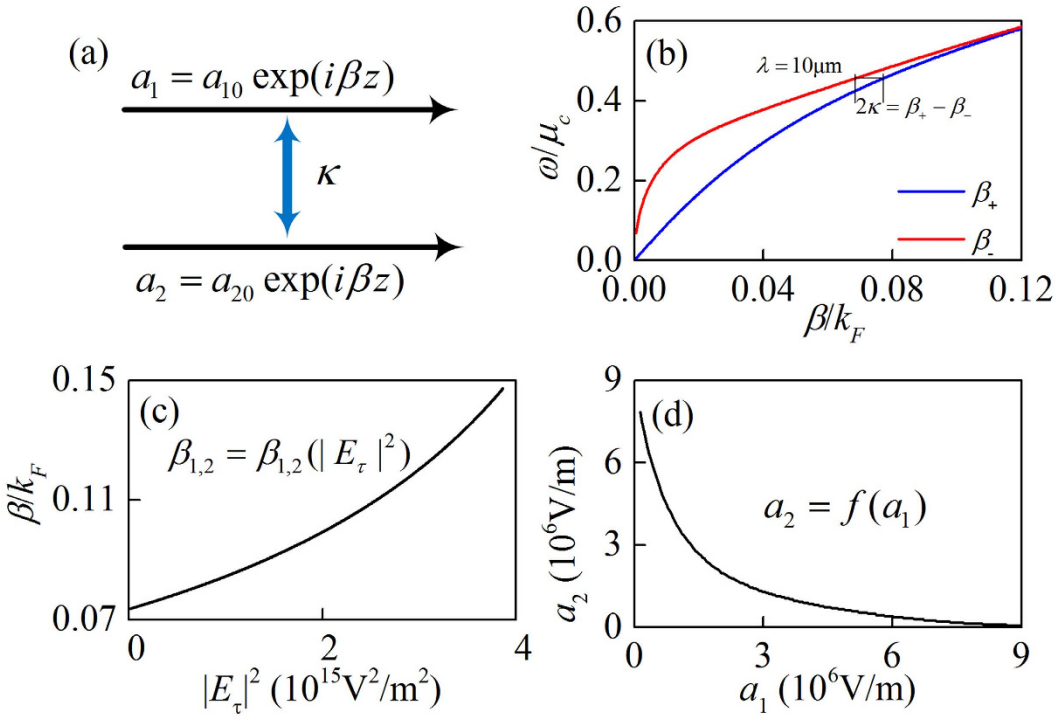

Figure 5. (**a**) The scheme of the coupling between two graphene waveguides. (**b**) The dispersion relations of the linear bi-graphene waveguide with distance *d*. (**c**) The nonlinear induced propagation constant change of a single graphene waveguide. (**d**) The third solution $a_2 = f(a_1)$ which satisfying Eq. (10) and Eq. (11).

treating $a_{1,2}$ as the tangential component of electrical field in amplitude, we obtain the coupled mode theory in nonlinear case

$$\begin{pmatrix} i\beta_1(|a_1+\gamma a_2|^2) & i\kappa \\ i\kappa & i\beta_2(|a_2+\gamma a_1|^2) \end{pmatrix}\begin{pmatrix} a_1 \\ a_2 \end{pmatrix} = \frac{\partial}{\partial z}\begin{pmatrix} a_1 \\ a_2 \end{pmatrix} \tag{9}$$

where $|a_1+\gamma a_2|^2$ and $|a_2+\gamma a_1|^2$ are the total field intensity with the similar meaning to the $|E_{1,\tau,+}|^2$ and $|E_{3,\tau,-}|^2$, respectively, and γ is an empiric factor related to β and *d*, which is fitted from the numerical data shown in Fig. 2. For propagation along the z direction ($\partial_z = i\beta$), a_1 and a_2 must satisfy Eq. (10) and Eq. (11) simultaneously

$$\beta = \beta_1(|a_{10}+\gamma a_{20}|^2) + \kappa a_{20}/a_{10} \tag{10}$$

$$\beta = \beta_2(|a_{20}+\gamma a_{10}|^2) + \kappa a_{10}/a_{20} \tag{11}$$

The first two solutions are $a_{20} = \pm a_{10}$, and the third one can be only obtained numerically shown in Fig. 5(d). Thus, $a_{20} = \pm a_{10}$ and $a_{20} = f(a_{10})$ represent three branches obtained from Eq. (10) (or Equation (11)). The theoretical result from the coupled mode theory in nonlinear case at a proper value of $\gamma \sim -0.07$is shown in Fig. 6. The relationship $|H_0| \sim |a_1+\gamma a_2|\omega\varepsilon_0\varepsilon_1/K_{x,1}$ can be used. It is found that the theoretical result consistent with the numerical one shown in Fig. 2.

The symmetric condition of $a_{20} = \pm a_{10}$ leads to the symmetric increase of β_1 and β_2, hence, equality $\beta_1 = \beta_2$ is always established. Corresponding branches are presented by black and red curves in Fig. 6 (and Fig. 2), i.e., symmetric and antisymmetric field distribution, respectively. For asymmetric condition $a_{10} > a_{20} > 0$ (or $a_{20} > a_{10} > 0$), the former term in Eq. (10) is larger (smaller) than that one in Eq. (11), but the latter term had an opposite order. When these two variation become equilibrium at $a_{20} = f(a_{10})$, we have the blue branch as shown in Fig. 6. We can conclude that the asymmetric mode come from the equilibrium of the propagation constant ($\beta_1(|a_{10}+\gamma a_{20}|^2)$) increase caused by the nonlinearity and compensation ($\kappa a_{20}/a_{10}$) due to the coupling.

Discussion

In summary, the coupled and dispersion properties of the graphene-dielectric-graphene structure are studied. The propagation constant is found to increase with the field intensity for both the symmetric and antisymmetric mode, whereas the antisymmetric mode splits off an asymmetric mode. When the nonlinearity of graphene is small ($\mu_c = 0.27$ eV, 0.22 eV), the dispersion relations shows three branches, and there is a fold-back point in each branch. Continuing to increase the nonlinearity of grapheme (decreasing μ_c to 0.19 eV), the fold-back point disappears and there is only one branch corresponding to the symmetric mode. By introducing the nonlinear

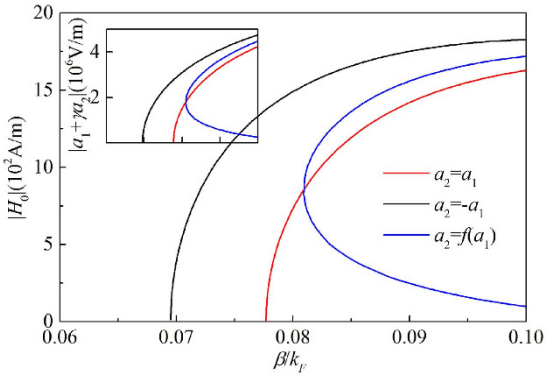

Figure 6. The initial magnetic field H_0 versus propagating constant β derived from nonlinear coupled mode theory after the transformation of $|a_{10}+\gamma a_{20}| \rightarrow |H_0|$. The inset is β vs. $|a_1+\gamma a_2|$ with $\kappa = 4.3 \times 10^{-3} k_F$ and $\gamma \sim -0.07$.

coupled mode theory, the features of the nonlinear plasmonic waveguide could be understood well. The reason for emergence of asymmetric mode is revealed. It is originated from the equilibrium of the propagation constant increase caused by the nonlinearity and the compensation due to the coupling.

References

1. Bonaccorso, F., Sun, Z., Hasan, T. & Ferrari, A. C. Graphene photonics and optoelectronics. *Nat. Photonics* **4,** 611–622 (2010).
2. Koppens, F. H. L., Chang, D. E. & García de Abajo, F. J. Graphene plasmonics: a platform for strong light matter interactions. *Nano Lett.* **11,** 3370–3377 (2011).
3. Grigorenko, A. N., Polini, M. & Novoselov, K. S. Graphene plasmonics. *Nat. Photonics* **6,** 749–758 (2012).
4. Low T. & Avouris, P. Graphene plasmonics for terahertz to mid-infrared applications. *ACS Nano* **8,** 1086–1101 (2014).
5. Emani, N. K., Kildishev, A. V., Shalaev, V. M. & Boltasseva, A. Graphene: A dynamic platform for electrical control of plasmonic resonance. *Nanophotonics*, **4,** 214–223(2015).
6. Christensen, J., Manjavacas, A., Thongrattanasiri, S., Koppens, F. H. L. & García de Abajo, F. J. Graphene Plasmon Waveguiding and Hybridization in Individual and Paired Nanoribbons. *ACS Nano* **6,** 431–440 (2012).
7. Wang, G., Liu, X., Lu, H. & Zeng. C. Graphene plasmonic lens for manipulating energy flow. *Scientific Reports* **4,** 4073 (2014).
8. Gu, X., Lin, I. T. & Liu, J. M. Extremely confined terahertz surface plasmon-polaritons in graphene-metal structures. *Appl. Phys. Lett.* **103,** 071103 (2013).
9. Yan, H. *et al.* Damping pathways of mid-infrared plasmons in graphene nanostructures. *Nat. Photonics* **7,** 394–399 (2013).
10. Gao, W. *et al.* Excitation and Active Control of Propagating Surface Plasmon Polaritons in Graphene. *Nano Lett.* **13,** 3698−3702 (2013).
11. Zhou, W. *et al.* Atomically localized plasmon enhancement in monolayer graphene. *Nat. Nanotechnology* **7,** 161–165 (2012).
12. Dai, Z. *et al.* Plasmon-driven reaction controlled by the number of graphene layers and localized surface plasmon distribution during optical excitation. *Light: Science & Applications* **4,** e342 (2015).
13. Chen, J. *et al.* Optical nano-imaging of gate-tunable graphene plasmons. *Nature* **487,** 77–81 (2012).
14. Fei, Z. *et al.* Gate-tuning of graphene plasmons revealed by infrared nano-imaging. *Nature* **487,** 82–85 (2012).
15. Constant, T. J., Hornett, S. M., Chang, D. E. & Hendry, E. All-optical generation of surface plasmons in graphene. *Nature Physics* **12,** 124–127 (2016).
16. Ni, G. X. *et al.* Ultrafast optical switching of infrared plasmon polaritons in high-mobility graphene. *Nat. Photonics* **10,** 244–247 (2016).
17. Zeng, C., Guo, J. & Liu, X. High-contrast electro-optic modulation of spatial light induced by graphene-integrated Fabry-Perot microcavity. *Appl. Phys. Lett.* **105,** 121103 (2014).
18. Zeng, C., Cui, Y. & Liu. X. Tunable multiple phase-coupled plasmon-induced transparencies in graphene metamaterials. *Opt. Express* **23,** 545–551 (2015).
19. Hanson, G. W. Quasi-transverse electromagnetic modes supported by a graphene parallel-plate waveguide. *J. Appl. Phys.* **104,** 084314 (2008).
20. Wang, B., Zhang, X., Yuan, X. & Teng, J. Optical coupling of surface plasmons between graphene sheets. *Appl. Phys. Lett.* **100,** 131111 (2012).
21. Wang, B., Zhang, X., García-Vidal, F. J., Yuan, X. & Teng, J. Strong coupling of surface plasmon polaritons in monolayer graphene sheet arrays. *Phys. Rev. Lett.* **109,** 073901 (2012).
22. Mikhailov, S. A. Non-linear electromagnetic response of graphene. *Europhys. Lett.* **79,** 27002 (2007).
23. Hendry, E., Hale, P. J., Moger, J., Savchenko, A. K. & Mikhailov, S. A. Coherent Nonlinear Optical Response of Graphene. *Phys. Rev. Lett.* **105,** 097401 (2010).
24. Gorbach, A. V. Nonlinear graphene plasmonics: amplitude equation for surface plasmons. *Physical Review A* **87,** 013830 (2013).
25. Nesterov, M. L., Bravo-Abad, J., Nikitin, A. Y., García-Vidal, F. J. & Martin-Moreno, L. Graphene supports the propagation of subwavelength optical solitons. *Laser Photonics Rev.* **7,** L7–L11 (2013).
26. Smirnova, D. A., Gorbach, I. V., Iorsh, I. V. Shadrivov, I. V. & Kivshar, Y. S. Nonlinear switching with a graphene coupler. *Phys. Rev. B* **88,** 045443 (2013).
27. Smirnova, D. A., Shadrivov, I. V., Smirnov, A. I. & Kivshar, Y. S. Dissipative plasmon-solitons in multilayer graphene. *Laser Photonics Rev.* **8,** 291–296 (2014).
28. Bludov, Y. V., Smirnova, D. A., Kivshar, Y. S., Peres, N. M. R. & Vasilevskiy, M. I. Discrete solitons in graphene metamaterials. *Phys. Rev. B* **91,** 045424 (2015).
29. Jablan, M., Buljan, H. & Soljačić, M. Plasmonics in graphene at infrared frequencies. *Phys. Rev. B* **80,** 245435 (2009).
30. Hwang E. H. & Das Sarma, S. Dielectric function, screening, and plasmons in two-dimensional graphene. *Phys. Rev. B* **75,** 205418 (2007).
31. Haus, H. A. *Waves and fields in optoelectronics* (Prentice-hall, 1984).
32. Mikhailov, S. A. & Ziegler, K. New electromagnetic mode in graphene. *Phys. Rev. Lett.* **99,** 016803 (2007).

Acknowledgements
This work was supported by the Program for Innovation Research of Science in Harbin Institute of Technology, the National Basic Research Program of China (Grants No.: 2013CB328702) and the Fundamental Research Funds for the Central Universities.

Author Contributions
X.Q.J. and H.M.Y. contributed equally to this work. X.Q.J. and H.M.Y. proposed the idea and performed numerical calculations. All authors contributed to the preparation and writing of the manuscript.

Additional Information
Competing financial interests: The authors declare no competing financial interests.

How to cite this article: Jiang, X. *et al.* Nonlinear plasmonic dispersion and coupling analysis in the symmetric graphene sheets waveguide. *Sci. Rep.* **6**, 39309; doi: 10.1038/srep39309 (2016).

Publisher's note: Springer Nature remains neutral with regard to jurisdictional claims in published maps and institutional affiliations.

This work is licensed under a Creative Commons Attribution 4.0 International License. The images or other third party material in this article are included in the article's Creative Commons license, unless indicated otherwise in the credit line; if the material is not included under the Creative Commons license, users will need to obtain permission from the license holder to reproduce the material. To view a copy of this license, visit http://creativecommons.org/licenses/by/4.0/

© The Author(s) 2016